Astrocyte-mediated disruption of ROS homeostasis in Fragile X mouse model

Gregory G. Vandenberg[1], Neal J. Dawson[2], Alison Head[1], Graham R. Scott[2], and Angela L. Scott[1]

[1]Department of Pathology and Molecular Medicine, McMaster University, 1200 Main St. West, Hamilton, Ontario L8N 3Z5, Canada; [2]Department of Biology, McMaster University, 1280 Main St. West, Hamilton, Ontario L8S 4K1, Canada

Running title: Astrocyte-mediated ROS dysregulation in FXS

Keywords: Fragile X Syndrome, astrocyte, mouse model, oxidative stress, mitochondrial respiration, reactive species, antioxidants

Number of words: Abstract: 217 words; Introduction: 847 words; Discussion: 1814 words

Number of figures: 5 (no color print required)

Address correspondence to:

Dr. Angela Scott

Department of Pathology and Molecular Medicine, McMaster University, 1200 Main St. West, Hamilton, Ontario L8N 3Z5, Canada

Tel: 905-525-9140, x20531

Email: <scottan@mcmaster.ca>

Acknowledgements: We sincerely thank Colin Nurse for his support and expert advice on this project. G. Scott, and A. Scott are funded by Natural Sciences and Engineering Research Council operating grants. The authors declare no competing financial interests.

Abstract

Astrocytes, glial cells within the brain, work to protect neurons during high levels of activity by maintaining oxidative homeostasis via regulation of energy supply and antioxidant systems. In recent years, mitochondrial dysfunction has been highlighted as an underlying factor of pathology in many neurological disorders. In animal studies of Fragile X Syndrome (FXS), the leading genetic cause of autism, higher levels of reactive oxygen species, lipid peroxidation, and protein oxidation within the brain indicates that mitochondria function is also altered in FXS. Despite their integral contribution to redox homeostasis within the CNS, the role of astrocytes on the occurrence or progression of neurodevelopmental disorders in this way is rarely considered. This study specifically examines changes to astrocyte mitochondrial function and antioxidant expression that may occur in FXS. Using the *Fmr1* knockout (KO) mouse model, mitochondrial respiration and reactive oxygen species (ROS) emission were analyzed in primary cortical astrocytes. While mitochondrial respiration was similar between genotypes, ROS emission was significantly elevated in *Fmr1* KO astrocytes. Notably, NADPH-oxidase 2 expression in *Fmr*1 KO astrocytes was also enhanced but only changes in catalase antioxidant enzyme expression were noted. Characterization of astrocyte factors involved in redox imbalance is invaluable to uncovering potential sources of oxidative stress in neurodevelopmental disorders and more specifically, the intercellular mechanisms that contribute to dysfunction in FXS.

Introduction

During development, oxidative homeostasis is highly regulated within the nervous system and a tight balance of free radicals is important for many developmental processes (reviewed in Salim, 2017). However, deviations of either the production or elimination of free radicals can result in oxidative stress associated with abnormal increases to reactive oxygen species (ROS) that lead to DNA damage, protein loss and lipid peroxidation (Cobley, Fiorello, & Bailey, 2018). Not surprisingly, several neurodevelopmental disorders have been linked to oxidative stress, including autism spectrum disorders (ASDs); with the degree of oxidative stress directly correlated to the severity of symptoms in some cases (Pangrazzi, Balasco, & Bozzi, 2020). In an animal model of Fragile X Syndrome (FXS), a genetic disorder highly comorbid with anxiety, hyperactivity and ASDs, higher levels of ROS have been measured in various brain tissues (el Bekay, et al., 2007; D'Antoni, et al., 2019). The pathology that underlies abnormalities in redox regulation in neurodevelopmental disorders like FXS remain unclear, but several reports have linked it to mitochondrial dysfunction within the CNS.

FXS is the most common inherited cause of intellectual disability and ASD that is caused by the instability of a CGG-repeated tract at the 5' end of the *Fmr*1 transcript, which leads to hypermethylation and silencing of FMRP (Fragile X mental retardation protein). FMRP functions as a translational regulator for several hundred downstream proteins and is associated with synaptic polyribosomes and RNA granules in neurons (Khayachi et al., 2018; Raspa, Wheeler, & Riley, 2017). In a recent study, impairment to mitochondrial fusion behaviour led to developmental deficits in newly formed FXS hippocampal neurons (Shen et al., 2019). They found that FMRP deficiency resulted in

a decrease in Hungtinin mRNA and protein levels within hippocampal neurons that led to a decrease in mitochondrial fusion gene expression, impaired mitochondrial fusion, and reduced dendritic complexity and maturation. While this work demonstrated mitochondrial dysfunction and the vulnerability of developing neurons in FXS, how this mutation affects other neural cell types that also rely on FMRP during brain development has not been studied. In the CNS, astrocytes play a significant role in regulating oxidative homeostasis, with the ability to either exacerbate oxidative stress via the production of ROS or modulate resistance via the secretion of antioxidants (Jou, 2008; Blanc et al., 1998). Astrocytes normally express FMRP throughout development and a lack of FMRP has led to various impairments to astrocyte function, including changes to glutamate uptake and catabolism (Higashimori, et al., 2016). One primary goal of this study was to examine the consequence of FMRP deletion on mitochondrial function and ROS emission in astrocytes in order to further elucidate their potential contribution to oxidative stress in FXS.

During periods of oxidative stress, the supply of astrocyte-mediated antioxidants is especially important for the protection of neurons susceptible to oxidative damage. One particularly key role of astrocytes is the synthesis and exportation of glutathione to neurons (Wilson, 1997). Glutathione (GSH) acts to detoxify ROS within the brain and deficiency of this tripeptide has been associated with mitochondrial damage and neurodegeneration (Jain et al., 1991; Bains & Shaw, 1997). Astrocytes not only produce high levels of GSH within the CNS but also supply neurons with the essential precursors for GSH synthesis (Dringen et al., 1999). Furthermore, in response to high or low levels of ROS, astrocytes can induce the expression of superoxide dismutase (SOD) or

nicotinamide adenine dinucleotide phosphate (NADPH) oxidase, respectively (Wang et al, 2018A). SOD is responsible for the dismutation of superoxide within the cytoplasm and mitochondria, converting superoxide (O_2-) produced from oxidative phosphorylation into oxygen (O_2) and hydrogen peroxide (H_2O_2), a less damaging form of ROS degraded by other enzymes (reviewed in Wang et al, 2018B). The expression of SOD in astrocytes appears particularly important to neuronal survival. In neuron-astrocyte co-cultures, approximately half of the neurons die when cultured with SOD-deficient astrocytes as compared with wild-types, and the surviving neurons show dramatic decreases of synaptic proteins in the presence of glutamate (Kunze et al., 2013). Given that excess glutamate has been associated with aberrant activity within the FXS brain, changes to SOD expression in astrocytes could act to exacerbate glutamate-mediated neuronal effects (Mahmoud et al, 2019).

In contrast to SOD, NADPH oxidase in astrocytes produces intracellular ROS needed for redox signalling. Notably, overproduction of ROS via NADPH oxidase has been noted in hyperactive circuits, and greater activation of NADPH oxidase in the *Fmr1* KO mouse brain has been previously reported (Wang et al, 2018A; el Bekay et al., 2007). Taken together, dysregulation of astrocyte-mediated antioxidant function in FXS may largely contribute to redox imbalance within the CNS and underscore many downstream consequences to neuronal circuitry. In light of this, our study examined several key enzymes involved in oxidative homeostasis within wild-type and *Fmr1* KO astrocytes in order to promote our understanding of glial-mediated pathophysiology in FXS.

Materials and Methods

Ethical Approval. Wildtype (WT) mice and *Fmr1* KO mice (background FVB.129P2[B6]-Fmr1tm1Cgr) were housed and bred in the McMaster University Central Animal Facility. All animal-handling procedures and experiments followed the guidelines set by the Canadian Council on Animal Care and were approved by the McMaster Animal Research Ethics Board (Animal Utilization Protocol 17-04-11).

Cortical Astrocyte Cell Culture. Each primary astrocyte culture was prepared from the combination of brain tissue dissected from 3-4 WT or *Fmr1* KO pups at P1-P3. The cortices were isolated from each brain and mechanically homogenized with a scalpel blade. The cortices were then combined and chemically homogenized in 2.5% Trypsin (Invitrogen Canada Inc., Burlington, ON, Canada) in the presence of DNase I (Roche, Penzburg, Upper Bavaria, Germany). After thorough trituration and passage through a cell strainer (70 μm; Thermo Fisher Scientific, Waltham, Massachusetts, United States), the cell suspension was centrifuged for 5 minutes at 1400 rpm. The supernatant was removed, and the pellet was resuspended in 20 mL of minimum essential media (MEM; Invitrogen) supplemented with 6% glucose and 10% horse serum (Invitrogen). The cell suspension was then placed in a T75 tissue culture flask and incubated at 37°C with 5% CO_2 approximately 12-14 days. Media changes of half volume glia media (10 mL; minimum essential media supplemented with 6% glucose and 10% horse serum) occurred 24 hours after plating and then every two to three days.

At 80-90% cell confluence, the media was replaced with 0.05% trypsin-EDTA and glial media and incubated for 5 minutes at 37° C. Following incubation, 5 mL of glial

media was added to the flask and the solution was repeatedly pipetted along the bottom of the flask to lift cells. All of the liquid suspension was removed and centrifuged at 200 rpm for 5 minutes. Each resulting pellet of cells was then used as one biological sample (n) and prepared for either respirometry measurements or protein assays as described below. Notably, no two replicates within any experiment were collected from cultured cells isolated from pups of the same litter. The sample number (n) is indicated for each experiment within the results section, as well as the individual figure legends.

The cells used for real-time respiration studies were resuspended in 1 mL of respiration buffer (in mM: 0.5 EGTA, 3 $MgCl_2$, 60 potassium lactobionate, 20 taurine, 10 KH_2PO_4, 20 Hepes, 110 sucrose, 1 g l−1 fatty acid-free bovine serum albumin; pH 7.1). After thorough trituration, the cells were counted via a haemocytometer and a Zeiss Axioimager M2 (x10) and were then immediately used for high resolution respirometry.

The cells collected for protein assays were resuspended in 1 mL of glial media. The cell suspension was then centrifuged again at 1400 rpm for 5 minutes. The supernatant was removed, and the pellet was flash-frozen in liquid nitrogen prior to storage at -80° C.

Mouse Genotyping. At the time of tissue collection, tail segments (0.5-1 cm in length) were also collected from the mice used for cell culture. A random selection of samples from each group were used to confirm the genotypes of the mice using PCR as previously described in Wallingford et al., (2017). Briefly, DNA extraction was completed using the Extract-N-Amp™ PCR Kit according to the manufacturer's instructions (catalog# XNAT2, Sigma-Aldrich). Prior to the PCR, the following primers were added to

each sample (with final primer concentrations of approximately 1 μM): CAC GAG ACT AGT GAG ACG TG (mutant forward; primer oIMR2060; Jackson Laboratory, Bar Harbor, ME, USA), TGT GAT AGA ATA TGC AGC ATG TGA (WT forward; primer oIMR6734; Jackson Laboratory), CTT CTG GCA CCT CCA GCT T (common; primer oIMR6735; Jackson Laboratory). PCR reaction conditions were equivalent to those outlined by Jackson Laboratory genotyping protocols for B6.129-Fmr1^{tm1Rbd}/J (http://jaxmice.jax.org/protocolsdb/f?p=116:2:::NO:2:P2_MASTER_PROTOCOL_ID,P2_JRS_CODE:4718,010504). Following PCR, the amplified DNA samples were run through a 2% agarose gel. Gels were imaged using SYBR Safe DNA Gel Stain (Invitrogen) and a ChemiDoc Imaging System (Bio-Rad) (data not shown).

Mitochondrial Respiration and ROS Emission. Respiration and ROS emission of 1 x 10^6 primary cortical astrocytes were measured simultaneously using high-resolution respirometry (Oxygraph-2K, Oroboros Instruments, Innsbruck, Austria) in 2 mL of respiration buffer (in mM: 0.5 EGTA, 3 $MgCl_2$, 60 potassium lactobionate, 20 taurine, 10 KH_2PO_4, 20 Hepes, 110 sucrose, 1 g l−1 fatty acid-free bovine serum albumin; pH 7.1) at 37°C. Respiration was measured from the rate of decline of O_2 concentration, while ROS emission was measured by the fluorescent detection of resorufin (excitation wavelength of 525 nm and AmR filter set, Oroboros Instruments). For simultaneous ROS detection, exogenous superoxide dismutase (22.5 U/mL), Ampliflu Red (15 μM) and horseradish peroxidase (3 U/mL; which catalyses the generation of resorufin from hydrogen peroxide and Ampliflu Red), was added to the respiration buffer. Exogenous H_2O_2 solutions were used to calibrate the resorufin signal, such that ROS emission rate

was measured as the molar rate of H_2O_2 appearance. After calibration, the 1 x 10^6 cells were added to a respirometry chamber and cells were permeabilized with the addition of digitonin (6 µM; Djafarzadeh and Jakob, 2017) to the respirometry chamber.

After a 5-minute acclimation, LEAK respiration was stimulated with the addition of 10 mM glutamate (Sigma-Aldrich, St. Louis, MO, USA) and 1 mM malate (Sigma-Aldrich) to the respirometry chamber and readings were recorded for approximately 2 minutes following every treatment. Multiple complexes of the electron transport system (during OXPHOS respiration in the presence of 10 mM glutamate and 1 mM malate) were stimulated via progressive additions of 5 mM ADP and 5 mM pyruvate (complex I; Sigma-Aldrich), 10 mM of succinate (complexes I + II; Sigma-Aldrich), and 2 mM of ascorbate and 0.5 mM of TMPD (complex IV; Sigma-Aldrich). After each addition of substrate, respiration rates and H_2O_2 emission rates were monitored and recorded until a stable steady state was reached (approximately 2 minutes). Each experiment lasted approximately 25 mins from time of the addition of Digitonin to the final respiration state measurement.

Microscopy. Primary cultured astrocytes labelled with Mitotracker Red CMXRos (Invitrogen) were imaged at 40x objective magnification using the Axio Observer Z1 inverted microscope, Axiocam 506 camera, and Zen Blue (2.0) Software (Zeiss; Oberkochen, Germany). Cells were plated onto coverslips precoated with Poly-D-Lysine (1 mg/mL; Sigma-Aldrich) and laminin (0.1 mg/mL; Invitrogen) at a density of 8000 cells per coverslip. Cells were maintained in minimum essential media with 6% glucose (Sigma-Aldrich) and 10% horse serum (Invitrogen) on coverslips for 7 days at 37°C.

Forty-five minutes prior to imaging, media was removed and the cells were incubated with 25 nM Mitotracker Red CMXRos (Invitrogen) in phosphate buffered saline (Gibco; Gaithersburg, MD, US). The dye solution was then removed and replaced by 1X PBS. Cells were then imaged immediately (40x, Axio Observer Z1) within an onstage incubation chamber maintained at 5% CO_2 and 37°C.

Enzyme Activity. Citrate synthase and cytochrome c oxidase activities were measured using a protocol adapted from Dawson et al. (2016). Previously prepared samples (cell culture pellets) were homogenized in 10 volumes of ice-cold homogenizing buffer A [100 mmol l^{-1} KH_2PO_4 buffer, pH 7.2, containing 0.1% triton x-100, 1 mmol l^{-1} EGTA, 1 mmol l^{-1} EDTA and 1 mmol l^{-1} phenylmethylsulfonyl fluoride (PMSF)]. Homogenates were then centrifuged at 1000 g at 4°C and the supernatant was collected for use in enzyme assays. The maximal activity for each sample was assayed at 37°C and measured in triplicate.

Enzyme activity was determined as the difference between the rate measured using all assay components and the background reaction rate. In the case of cytochrome c oxidase, the background reaction rate is the oxidation rate of cytochrome c (oxidized) and for citrate synthase it is the reaction rate without oxaloacetate. Measurements were carried out in 100 mmol l^{-1} KH_2PO_4 (pH 7.2) under the following assay conditions: 0.2 mmol l^{-1} reduced cytochrome c (Calzyme Laboratories) (molar extinction coefficient (ε)=28.5 (mmol l^{-1})$^{-1}$ cm^{-1} at 550 nm) for cytochrome c oxidase [complex IV of the electron transport system (CIV)]; and 0.5 mmol l^{-1} oxaloacetate, 0.15 mmol l^{-1} acetyl-coA, 0.15 mmol l^{-1} 5,5′- dithiobis-2-nitrobenzoic acid (ε=14.15 (mmol l^{-1}

248 $)^{-1}$ cm^{-1} at 412 nm) for citrate synthase of the tricarboxylic acid cycle (CS). Units of
249 enzyme activity were expressed as the conversion of µmol substrate/cell/minute. All
250 substrates were added in saturating concentrations as determined prior to experimental
251 measurements. Assays were measured using an xMark Microplate Spectrophotometer
252 (Biorad, Mississauga, ON, CAN). Data were analyzed using the accompanying
253 Microplate Manager Software and GraphPad Prism 6 (GraphPad Software, La Jolla,
254 CA, USA). Biochemicals were supplied by Sigma-Aldrich unless otherwise stated.
255
256 ***Western Blotting.*** Standard DC protein assays were performed on each cell culture
257 sample in order to standardize protein content used for western blotting. RIPA buffer
258 was made by adding one tablet of protease inhibitor (Roche) and one tablet of
259 phosphatase inhibitor (Roche) to 10 mL of the stock solution, which was kept on ice.
260 Once defrosted, the samples were centrifuged at 10,000 rpm for 3 minutes at 4° C.
261 Supernatant was removed and the pellets were mechanically homogenized in 20 µL of
262 RIPA buffer with a Teflon pestle for several minutes. The homogenate was chilled on
263 ice for 15 minutes, prior to centrifugation at 10,000 rpm for 10 minutes at 4° C. The
264 supernatant was removed and transferred to a new tube and stored on ice until use in
265 the DC protein assay. As previously reported (Wallingford et al., 2017), we prepared a
266 standard curve consisting of serial dilutions of bovine serum albumin (BSA; Sigma-
267 Aldrich, cat. no. A-7906) and prepared the standards and samples per manufacturer's
268 instructions (Bio-Rad, Hercules, CA, USA). Plates were gently shaken for 15 minutes
269 prior to spectrophotometer readings (xMark Microplate Absorbance Spectrophotometer,

Bio-Rad) taken at 750 nm. Samples were flash frozen in liquid nitrogen and stored at -80° C until further use.

After the amount of protein in each sample was determined, 30 µg of protein from each sample was combined with sample buffer: 2x Laemmli Buffer (Bio-Rad) and 5% 2-Mercaptoethanol (Sigma-Aldrich). Samples were heated for 5 minutes at 95°C, centrifuged briefly, and loaded onto a gradient 4-15% precast polyacrylamide stain-free gel (Bio-Rad).

All experimental samples were aliquoted and prepared for Western blotting with the addition of 2x Laemmli Buffer (Bio-Rad) and 5% 2-Mercaptoethanol (Sigma-Aldrich). Samples were heated for 5 minutes at 95°C, centrifuged briefly, and 30 µg of protein from each sample were loaded onto a gradient 4-15% precast polyacrylamide stain-free gel (Bio-Rad). Electrophoretic separation of proteins was done at 125V for 1 hour in a solution of 1X Tris-Glycine SDS running buffer (Bio-Rad). After electrophoresis, the gels were activated with UV light (302 nm) for 1 minute and then transferred onto polyvinyl difluoride membranes (Bio-Rad) using the Trans-Blot Turbo Transfer System (Bio-Rad). The membranes were placed in a 1X tris buffered saline and Tween-20 solution (TBS-T) and then imaged for total protein using a ChemiDoc Imaging System (Bio-Rad). Membranes were then incubated in a 5% non-fat milk solution in TBS-T for 1 hour at room temperature. Following this, membranes were rinsed with TBS-T and then incubated overnight at 4°C with TBS-T containing one of the following primary antibodies: anti-superoxide dismutase 1 (anti-SOD-1; rabbit; 1:5000; Abcam; ab13498), anti-SOD2/MnSOD (rabbit; 1:5000; Abcam; ab13533), anti-glutathione peroxidase 1 (anti-GPx; rabbit; 1:1000; Abcam; ab22604), anti-glutathione reductase (anti-GR; rabbit;

1:2000; Abcam; ab16801), anti-catalase (anti-CAT; rabbit; 1:2000; Abcam; ab16731), anti-nicotinamide adenine dinucleotide phosphate hydrogen (anti-NADPH) oxidase 2 (NOX2; rabbit; 1:5000; Abcam; ab129068), and anti-NADPH oxidase 4 (NOX4; rabbit; 1:500; Novus Biologicals; NB110-58851SS). Membranes were washed for 3 x10 minutes in TBS-T at room temperature, then incubated for 1 hour in horseradish peroxidase conjugated antibody (anti-rabbit, 1:2500, catalogue #: NA934-1ML; GE Healthcare Life Sciences, Mississauga, ON, CA). Membranes were washed for 3 x 10 minutes in TBS-T, then developed in the dark for 5 minutes using enhanced chemiluminesence developer (Bio-Rad) and imaged. Analysis of relative densitometry was done using Image Lab Software 5.2 (Bio-Rad) and bands of interest were normalized to total protein as well as a positive cross gel control. Normalized densitometry values were expressed relative to WT values.

Statistical Analyses. Statistical analyses were conducted using Prism (version 6, GraphPad Software, RRID: SCR_002798). Each N represented the number of independent culture preparations. For comparisons of two groups alone, two-tailed unpaired t tests were performed. For multiple comparisons the groups were compared using Two-way ANOVA and Tukey's multiple comparisons were used to determine effects of genotype or respiration state for each parameter. Data were presented as mean ± SEM. $P < 0.05$ was considered to be statistically significant.

Results

Elevated ROS emission in Fmr1-KO cortical astrocytes

High resolution respirometry of permeabilized cortical primary astrocytes was used to determine respiratory capacities across multiple mitochondrial electron transport complexes during both oxidative phosphorylation (OXPHOS) and leak state respiration. Respiration capacity of permeabilized cortical primary astrocytes in the *Fmr*1 KO mice (n=12) was similar to that of WT mice (n=12) during OXPHOS (*green section*, Fig. 1A), as the main effect of genotype in two-way ANOVA was not significant (P=0.395) across all OXPHOS respiration states: stimulation via ADP, glutamate, malate (P_{GM}), followed by maximal stimulation of Complex I with pyruvate (P_{GMP}), and maximal stimulation of Complexes I and II with succinate (P_{GMPS}) (Fig. 1C). Maximal stimulation of Complex IV using ascorbate and TMPD (P_{Tm}) was also similar between genotypes (P=0.136) (Fig. 1D). Leak respiration (L_N; *red section*, Fig. 1A) fuelled by glutamate and malate, prior to the addition of ADP, to stimulate oxidative phosphorylation was also similar in *Fmr*1 KO cortical astrocytes compared to WT (pairwise comparison, P=0.0402; Fig. 1B), despite the appearance of an upward trend.

During respiration, ROS emission from permeabilized cortical astrocytes was significantly elevated in *Fmr*1 KO (n=9) mice compared to WT (n=11) mice (Fig. 2). ROS emission varied as expected between respiration states, as reflected by the significant main effect of respiration state in two-way ANOVA ($P < 0.0001$). There was also a significant main effect of genotype on ROS emission (P=0.023), primarily driven by higher rates of ROS emission in *Fmr*1 KO (n=9) compared to WT (n=11) in the leak state (L_N) and during submaximal OXPHOS respiration *via* complex I (P_{GM}).

In order to assess possible genotypic differences in cellular mitochondrial content or distribution within astrocytes, we utilized both fluorescent microscopy and

mitochondrial enzyme assays to examine this. Notably, there were no observable differences in *Fmr1* KO and WT astrocyte mitochondrial content or distribution visualized with Mitotracker Red CMXRos (representative images shown in Fig. 3A-B). In addition, analysis of citrate synthase (CS) activity, a commonly used and validated biomarker for mitochondrial density (Vigelsø, Andersen, and Dela, 2014), showed *Fmr1* KO astrocytes with nearly equivalent activity levels as WT astrocytes (P=0.8923; Fig. 3C). We also found genotypic similarities in the activity of Cytochrome c oxidase (complex IV), a marker of mitochondrial cristae surface density, across *Fmr1* KO (5.10 ±0.43 fmol/cell/min; n=9) and WT (4.64 ±0.39 fmol/cell/min; n=8) astrocytes (P=0.4474; data not shown).

Greater NADPH-Oxidase expression in Fmr1-KO cortical astrocytes

Another common source of ROS production within astrocytes is NADPH oxidase (NOX), and we compared the expression of two primary NADPH-oxidase isoforms (NOX2 and 4) in WT and *Fmr1* KO primary cortical astrocytes. We found that the protein abundance of NOX2 was elevated in *Fmr1* KO (n=8) cultured cortical astrocytes compared to WT (n=7) astrocytes (130.8 ± 8.47% of WT; P<0.05; Fig. 4A). In contrast, we found that the expression levels for NOX4 were similar in cultured cortical astrocytes across *Fmr1* KO (n=8) and WT (n=8) mice (113.0 ± 32.26% of WT; P=0.7938; Fig. 4B). Both isoforms were expressed in cultured cortical astrocytes; however, abundance of full-length NOX2 appeared significantly greater than NOX4 (relative intensity per µg of protein; left panels Figure 4A-B). Overall, we found an elevation of NOX2 in *Fmr1* KO cultured cortical astrocytes along with no differences in expression of NOX4.

362

363 ***Relatively similar antioxidant levels in Fmr1-KO and WT cortical astrocytes***

364 We investigated the relative abundance of various key antioxidant enzymes in
365 astrocytes. The primary enzymes of the antioxidant system in astrocytes are highlighted
366 in Figure 5A. Protein expression of each enzyme was evaluated in primary cortical
367 astrocytes isolated from either *Fmr1* KO or WT mice (Fig. 5 and 6).

368 *Catalase (CAT)*

369 CAT, an enzyme responsible for the conversion of hydrogen peroxide to water,
370 reduces oxidative damage caused by ROS in astrocytes (Fig. 5A). Here we found a
371 moderate, yet significant, elevation of CAT in cultures isolated from *Fmr1* KO (n=7) mice
372 compared to those from WT mice (n=7) (157.1 ± 6.66% of WT; $P<0.05$; Fig. 5B). CAT
373 expression in postnatal astrocytes appeared relatively weak in both genotypes in
374 comparison to the levels of other antioxidant enzymes.

375 *Superoxide Dismutase 1 and 2 (SOD)*

376 Another important enzyme in the antioxidant system is superoxide dismutase
377 (SOD). There are two different polymorphisms of this enzyme within the cell: the Cu/Zn-
378 SOD (SOD1) enzyme located within the cytosol, and Mn-SOD (SOD2) enzyme found
379 within the mitochondria (Fig. 6A). The expression level of SOD1 in *Fmr1* KO primary
380 cortical astrocytes (n=7) was similar to expression levels in WT astrocytes (n=7) (105.8
381 ± 14.76% of WT; $P=0.8287$; Fig. 6A). Similarly, the expression of SOD2 in *Fmr1* KO
382 (n=7) cortical astrocytes was also similar to that of WT astrocytes (n=7) (95.4 ± 16.45%
383 of WT; $P=0.8305$; Fig. 6B).

384 *Glutathione Cycle Enzymes*

Within the glutathione cycle, glutathione peroxidase (GPx) works with glutathione reductase (GR) to catalyze hydrogen peroxide to water and drives the detoxification of lipid hydroperoxides (Fig. 5A). We found similar expression levels of GPx in primary cortical astrocytes (*Fmr1* KO, n=8; WT, n=7; *P*=0.7964) between genotypes (Fig. 6C). Similarly, the expression levels of GR in *Fmr1* KO primary cortical astrocytes (n=8) were comparable to that of WT astrocytes (n=8) (108.3 ± 23.79% of WT; *P*=0.8234; Fig. 6D). Notably, all SOD and glutathione antioxidant enzymes that we investigated were highly expressed in both WT and *Fmr1* KO cultured cortical primary astrocytes; however, no genotypic differences were observed.

Discussion

In this study, we measured the mitochondrial respiration of primary cortical astrocytes isolated from WT and *Fmr1* KO mice to assess oxygen flux during leak and oxidative phosphorylation (OXPHOS) across mitochondrial electron transport complexes. The OXPHOS capacity of the *Fmr1* KO astrocytes was overwhelmingly similar to that of WT astrocytes across successive stimulation of complexes I, II and IV, as well as leak respiration. Simultaneous readings of ROS emission also showed elevated levels in *Fmr1* KO astrocytes compared to WT astrocytes, particularly during leak and submaximal OXPHOS respiration *via* complex I. Interestingly, there were few genotypic differences in the overall expression of enzyme antioxidants that would offset the increase in mitochondrial ROS emission in *Fmr1* KO astrocytes. There was, however, significant increases to the expression of NADPH oxidase 2, *NOX2,* in *Fmr1* KO astrocytes that could further augment ROS levels in these cells. Collectively, our

results demonstrate that an imbalance between ROS production and elimination potentiates oxidative stress in *Fmr1* KO cortical astrocytes and that aberrant astrocyte activity contributes to redox imbalance within the FXS brain.

Oxidative stress pathology has been associated with a growing number of neurodevelopmental and neurodegenerative diseases. It is perhaps not surprising that enhanced levels of free radicals, as well as increased hydrogen peroxide production and lipid peroxidation activity were identified in brain homogenates of young adult *Fmr1* KO mice (el Bekay, et al., 2007; de Diego-Otero et al., 2009). In conjunction with this, systemic treatment of these mice with an antioxidant/radical scavenger, α-Tocopherol, effectively reversed the appearance of oxidative stress markers in a dose-dependent manner (de Diego-Otero et al., 2009). During development, synaptic transmission and dendritic spine development are highly dependent on mitochondrial morphology and bioenergetics (Flippo and Strack, 2017). In FXS, both synaptic function and dendritic spine maturation are impaired, an effect partially attributed to reductions of mitochondrial membrane potential and fusion dynamics in *Fmr1* KO neurons (Shen et al., 2019). Indeed, ROS overproduction in *Drosophila* leads to mitochondrial dysfunction and overall synaptic reduction within the CNS (Beckhauser, Francis-Oliveira, & De Pasquale et al., 2016), both of which have been noted in the FXS animal model. Interestingly, dendritic morphology of *Fmr1* KO neurons is largely normalized by the presence of WT astrocytes and induced in WT neurons by *Fmr1* KO astrocytes, suggesting a prominent role for astrocytes in FXS (Jacobs and Doering, 2010). Given the responsibility of astrocytes in protecting the neuronal microenvironments from

oxidative stress within the brain, exploration of astrocyte redox regulation in FXS warranted further investigation.

Astrocytes have a broad antioxidant response that clears free radicals produced within the CNS; however, they are also a source of ROS and when emission exceeds the detoxifying capacity, oxidative damage can ensue (Chen et al., 2020). Elevated levels of ROS are associated with reactive astrogliosis, a process of morphological and functional change that astrocytes undergo in response to CNS stress or damage. Astrocytes within this reactive state for prolonged periods are known to sustain high levels of ROS production, secrete proinflammatory molecules and promote neurotoxicity (reviewed in Rizor et al., 2019). Markers used to characterize reactive astrogliosis, such as glial fibrillary associated protein and pro-inflammatory tumor necrosis factor 2, are both elevated across several regions of the *Fmr1* KO brain (Yuskaitis, Beurel and Jope, 2010; Pacey et al., 2015). In addition, *Fmr1* KO astrocytes grown in isolation express enhanced levels of inflammatory induction factors, namely tenascin C and interleukin-6 (Krasovska and Doering, 2018). The significant elevations of ROS emission in *Fmr1* KO cortical astrocytes observed here suggest that astrocytes within the FXS brain have a higher degree of reactivity and contribute to the oxidative pathogenesis of this disease.

During normal conditions, the source of free radicals within astrocytes is primarily due to the mitochondria and the NOX pathway. The mitochondria are the greatest source of ROS in astrocytes and ROS production is largely dependent on the function of the mitochondrial respiratory chain (MRC), particularly complex I during OXPHOS (Zhao, Jiang, Zhang, and Yu, 2019). Interestingly, the MRC of astrocytes is markedly different than neurons, which depend on OXPHOS for ATP production. In neurons,

complex I is predominantly assembled into supercomplexes that support higher mitochondrial respiration with low ROS production (Bianchi et al., 2004). In contrast, the abundance of free, non-bound complex I is higher in astrocytes, and directly correlates with higher ROS production by comparison (Lopez-Fabuel et al., 2016). Whether MRC organization is altered in FXS is unknown, but inefficient MRC complex activity and compromised ATP production in the cerebral cortex of *Fmr1* KO mice has been reported (D'Antoni et al., 2019). Notably, the difference of ROS emission rate in the *Fmr1* KO astrocytes was not likely due to differences in mitochondrial volume or cristae surface density given the similarities in citrate synthase and cytochrome c oxidase activities between *Fmr1* KO and WT astrocytes, nor to changes in mitochondrial organization since distribution was comparable between genotypes.

The NADPH-oxidase pathway is another important source of ROS production within astrocytes. This family of enzymes contains 7 members, with NOX2 and 4 being the most abundant in the CNS (Sorce et al., 2017). Within the cell, NOX enzymes are located in the plasma membrane, as well as membranes of cellular organelles, including the endoplasmic reticulum and endosomes. Both NOX2 and 4 are expressed by astrocytes to varying degrees at rest but increase in expression and activity in response to stress. For instance, NOX2 levels are elevated during astrogliosis and is significantly upregulated by increasing levels of amyloid-β observed in Alzheimer's disease (Chay et al., 2017). Other stresses, such as lipopolysaccharide exposure or hypo-osmotic swelling, also lead to substantial increases of ROS production via NOX activation in astrocytes (Reinehr et al., 2007). Previous studies have reported greater generalized NADPH-oxidase activity within *Fmr1* KO brain tissue (el Bekay, et al., 2007), and our

476 results suggest that this arises at least partly from greater expression of NOX2 in
477 astrocytes. The lack of differences between NOX4 in *Fmr1* KO and WT astrocytes
478 suggests that NOX2 may be solely responsible for any differences in FXS.
479 In the healthy CNS, astrocytes also employ several mechanisms of
480 neuroprotection during excitatory transmission. Glutamate is the primary excitatory
481 neurotransmitter within the CNS, but if high amounts remain within the synaptic cleft,
482 overactivation of ionotropic glutamate receptors leads to calcium overload, generation of
483 ROS and neurotoxicity (Reynolds and Hastings, 1995). As a defence, astrocytes
484 actively transport glutamate out of the cleft via the glutamate transporters GLAST, GLT-
485 1 and EAAC1. Expression of GLT-1 in particular is significantly reduced in FMRP
486 deficient astrocytes, which leads to impaired glutamate uptake and enhanced neuronal
487 excitability within the somatosensory cortex (Higashimori et al., 2013; 2016). Astrocytes
488 also protect neurons via a robust antioxidant system that uses several different
489 enzymes to neutralize hydrogen peroxide within the synaptic zone. Given the reduction
490 of GLT-1 and the increase in ROS, we anticipated the antioxidant system to be
491 enhanced in *Fmr1* KO astrocytes.
492 Astrocytes are the primary source of glutathione, which acts in conjunction with
493 glutathione peroxidase (GPx) to catalyse the reduction of hydrogen peroxide and
494 peroxide radicals (Harvey et al., 2009). A previous report found that expression and
495 activity of glutathione peroxidase was significantly reduced in 4-month-old *Fmr*1 KO
496 mice brains (El Bekay et al. 2007). In contrast, we found that the expression of GPx or
497 glutathione reductase (GR), the enzyme that reduces glutathione disulfide to
498 glutathione, were not altered in *Fmr*1 KO astrocytes in comparison to WT. It may be that

dysregulation of GPx only occurs at later time points in development since differences between *Fmr1* KO and WT brain tissue have not been found in early postnatal stages (el Bekay et al., 2007).

Other key antioxidant enzymes regulated by ROS levels are catalase and superoxide dismutase (SOD). Interestingly, we did find that the expression of catalase was significantly elevated in *Fmr1* KO astrocytes in comparison to WT cells. Catalase, an enzyme responsible for the reduction of hydrogen peroxide, is found in relatively low abundance within the cytoplasm and peroxisomes in the mammalian brain (Mavelli et al., 1982). Given the low expression of catalase at that age, the increase of catalase expression observed within *Fmr1* KO astrocytes did not appear to be sufficient to effectively overcome ROS production observed here. The superoxide dismutase (SOD) polymorphisms, Cu-Zn and Mn-SOD (SOD1 and SOD2, respectively) work upstream to many of the other antioxidant enzymes to neutralize superoxides into hydrogen peroxide and O_2^-, which are then reduced by catalase and others. Both forms are expressed widely within the CNS, SOD1 being within the cytosol and SOD2 in the mitochondria. FMRP is known to regulate the translation of SOD1 protein within the brain, and expression of SOD1 was reported to be reduced in several brain regions of postnatal *Fmr1* KO mice compared to WT (Bechara et al., 2009). Since FMRP expression is normally quite high within the early postnatal brain, we were surprised by the similarities of SOD1 and 2 within the WT and *Fmr*1 KO astrocytes. This suggests that while FMRP may be an important regulator of SOD1, other regulatory factors appear to compensate for the loss of FMRP expression in *Fmr1* KO astrocytes.

Conclusions

While the study of possible mitochondrial or OXPHOS perturbations in isolated astrocytes is advantageous to understand changes due to the genetic variation in this cell type, future studies examining these relationships *in vivo* will help determine the degree to which it contributes to oxidative stress in FXS. For instance, the metabolic demand on astrocytes is greatly enhanced during neuronal activity and the fact that mitochondrial respiration is significantly higher in permeabilized tissue compared to cell preparations (Schopf et al., 2016; Van Bergen et al., 2014), it is likely that basal mitochondrial respiration and ROS emission is largely underestimated in our study. This, and the abnormal level of activation noted in *Fmr1*$^{-/-}$ cortical neurons (Bülow et al., 2019), may underscore some of the key differences that we found in our primary cells compared to studies examining cortical tissue of these mice.

Overall, our observations compliment previous studies in this area and point to a pivotal role of oxidative imbalance in the pathology of FXS. We show that changes to astrocyte-mediated ROS emission may in fact contribute to the loss of oxidative homeostasis within the FXS cortex, rather than prevent it via the antioxidant system. This study not only identifies novel pathophysiology associated with glial cell biology in FXS, but also highlights the need for innovative therapeutic strategies that target factors triggering oxidative stress in FXS and related neurological disorders.

References

Bains, J. S., & Shaw, C. A. (1997). Neurodegenerative disorders in humans: the role of glutathione in oxidative stress-mediated neuronal death. *Brain research reviews, 25*(3), 335-58.

Bechara, E. G., Didiot, M. C., Melko, M., Davidovic, L., Bensaid, M., Martin, P., . . . Bardoni, B. (2009). A Novel Function for Fragile X Mental Retardation Protein in Translational Activation. *PLoS Biology, 7*(1), e1000016.

Beckhauser, T. F., Francis-Oliveira, J., & De Pasquale, R. (2016). Reactive Oxygen Species: Physiological and Physiopathological Effects on Synaptic Plasticity. *Journal of Experimental Neuroscience, 10*(Suppl 1), 23-48.

Bianchi, K., Rimessi, A., Prandini, A., Szabadkai, G., & Rizzuto, R. (2004). Calcium and mitochondria: mechanisms and functions of a troubled relationship. *Biochimica et biophysica atca, 1742*(1-3), 119-31.

Blanc, E. M., Keller, J. N., Fernandez, S., & Mattson, M. P. (1998). 4-hydroxynonenal, a lipid peroxidation product, impairs glutamate transport in cortical astrocytes. *Glia, 22*(2), 149-60.

Brookes, P. S. (2005). Mitochondrial H+ leak and ROS generation: An odd couple. *Free Radical Biology and Medicine, 38*(1), 12-23.

Bülow, P., Murphy, T. J., Bassell, G. J., & Wenner, P. (2019). Homeostatic Intrinsic Plasticity Is Functionally Altered in Fmr1 KO Cortical Neurons. *Cell Reports*, *26*(6), 1378-1388.e3. https://doi.org/https://doi.org/10.1016/j.celrep.2019.01.035

Chay, K., Koong, K., Hwang, S., Kim, J., & Bae, C. (2017). NADPH Oxidase Mediates β-Amyloid Peptide-Induced Neuronal Death in Mouse Cortical Cultures. *Chonnam medical journal, 53*(3), 196-202.

Chen, Q., Huang, J., Tang, X., Liu, C., Huang, K., et al. (2020) The role of astrocytes in oxidative stress of central nervous system: A mixed blessing. *Cell Proliferation, 53(3)*, e12781.

Cobley, J. N., Fiorello, M. L., & Bailey, D. M. (2018). 13 reasons why the brain is susceptible to oxidative stress. *Redox Biology, 15*, 490-503.

Coyle, J. T., & Puttfarcken, P. (1993). Oxidative Stress, Glutamate, and Neurodegenerative Disorders. *Science, 262*, 689-695.

Cuadrado, A., Gimenez-Liorente, D., Kojic, A., Gomez-Lopez, G., Marti-Renom, M., & Losada, A. (2019). Specific Contributions of Cohesin-SA1 and CohesinSA2 to TADs and Polycomb Domains in Embryonic. *Cell Press, 27*, 3500-3510.

D'Ambrosia, M., Guerriero, A., Debitus, C., Ribes, O., Pusset, J., Leroy, S., & Pietra, F. (1993). Agelastatin A, a new skeleton cytotoxic alkaloid of the oroidin family. Isolation from the axinellid sponge Agelas dendromorpha of the coral sea. *Journal of Chemical Society*(16), 1305-1306.

D'Antoni, S., De Bari, L., Valenti, D., Borro, M., Bonaccorso, C. M., Simmaco, M., . . . Catania, M. V. (2019, January 1). Aberrant mitochondrial bioenergetics in the cerebral cortex of the Fmr1 knockout mouse model of fragile X syndrome. *Journal of Biological Chemistry*. doi:https://doi.org/10.1515/hsz-2019-0221

de Diego-Otero, Y., Romero-Zerbo, Y., el Bekay, R., Decara, J., Sanchez, L., Rodriguez-de Fonseca, & del Arco-Herrera, I. (2009). a-Tocopherol Protects

Against Oxidative Stress in the Fragile X Knockout Mouse: an Experimental Therapeutic Approach for the Fmr1 Deficiency. *Neuropyschopharmacology, 34*, 1011-1026.

Dringen, R., Pfeiffer, B., & Hamprecht, B. (1999). Synthesis of the Antioxidant Glutathione in Neurons: Supply by Astrocytes of CysGly as Precursor for Neuronal Glutathione. *Journal of neuroscience, 19*(2), 562-569.

el Bekay, R., Romero-Zerbo, Y., Decara, J., Sanchez-Salido, L., Del Arco-Herrar, I., Rodriguez-de Fonseca, F., & de Diego-Otero, Y. (2007). Enhanced markers of oxidative stress, altered antioxidants and NADPH-oxidase activation in brains from Fragile X mental retardation 1-deficient mice, a pathological model for Fragile X syndrome. *Europena Journal of Neuroscience, 26*, 3169-3180.

Flippo, K. H., & Strack, S. (2017). Mitochondrial dynamics in neuronal injury, development and plasticity. *Journal of cell science, 130*(4), 671-681.

Gnaiger. (2014). *Mitochondrial pathways and respiratory control. An introduction to OXPHOS analysis. 4th ed.* Innsbruck: Oroboros MiPNet Publications.

Gray , S., & Jandeleit-Dahm, K. (2015). The role of NADPH oxidase in vascular disease–hypertension, atherosclerosis & stroke. *Current pharmaceutical design, 21*, 5933-5944.

Griffiths, K. K., Wang, A., Wang, L., Tracey, M., Kleiner, G., Quinzii, C. M., . . . Levy, R. J. (under review). Inefficient Thermogenic Mitochondrial Respiration Due to Futile Proton Leak in a Mouse Model of Fragile X Syndrome. *Cell Press*.

Harvey, C., Thimmulappa, R., Singh, A., Blake, D., Ling, G., Wakabayashi, N., . . . Biswal, S. (2009). Nrf2-regulated glutathione recycling independent of

biosynthesis is critical for cell survival during oxidative stress. *Free radical biology & medicine, 46*(4), 443-53.

Herrera, F., Sainz, R. M., Mayo, J. C., Martin, V., Antolin, I., & Rodriguez, C. (2008). Glutamate induces oxidative stress not mediated by glutamate receptors or cystine transporters: protective effect of melatonin and other antioxidants. *Journal of Pineal Research*.

Higashimori, H., Schin, C. S., Chiang, M. S., Morel, L., Shoneye, T. A., Nelson, D. L., & Yang, Y. (2016). Selective Deletion of Astroglial FMRP Dysregulates Glutamate Transporter GLT1 and Contributes to Fragile X Syndrome Phenotypes In Vivo. *Journal of Neuroscience, 36*(27), 7079-94.

Jacobs, S. & Doering, L. (2010) Astrocytes prevent abnormal neuronal development in the fragile X mouse. *Journal of Neuroscience, 30 (12)*, 4508-14.

Jain, A., Martensson, J., Stole, E., Auld, P. A., & Meister, A. (1991). Glutathione deficiency leads to mitochondrial damage in brain. *Proceedings of the National Academy of Sciences of the United States of America, 88*(5), 1913-1917.

Jou, M.-J. (2008). Pathophysiological and pharmacological implications of mitochondria-targeted reactive oxygen species generation in astrocytes. *Advanced drug delivery reviews, 60*(13-14), 1512-26.

Khayachi, A., Gwizdek, C., Poupon, G., Alcor, D., Chafi, M., Casse, F., . . . Martin, R. (2018). Sumoylation regulates FMRP-mediated dendritic spine elimination and maturation. *Nature communications, 9*(1), 757.

Korge, P., Honda, H. M., & Weiss, J. N. (2003). Effects of fatty acids in isolated mitochondria: implications for ischemic injury and cardioprotection. *American Journal of Physiology. Heart and Circulatory Physiology, 285*(1), H259-69.

Krasovska, V., & Doering, L. (2018). Regulation of IL-6 Secretion by Astrocytes via TLR4 in the Fragile X Mouse Model. *Frontiers in molecular neuroscience, 11*, 272.

Kunze, A., Lengacher, S., Dirren, E., Aebischer, P., Magistretti, P. J., & Renaud, P. (2013). Astrocyte–neuron co-culture on microchips based on the model of SOD mutation to mimic ALS. *Integrative biology, 5*, 964-975.

Liemburg-Apers, D. C., Willems, P., Koopman, W., & Grefte, S. (2015). Interactions between mitochondrial reactive oxygen species and cellular glucose metabolism. *Archives of Toxicology, 89*, 1209-1226.

Lopez-Fabuel, I., Le Douce, J., Logan, A., James, A. M., Bonvento, G., Murphy, M., . . . Bolanos, J. (2016). Complex I assembly into supercomplexes determines differential mitochondrial ROS production in neurons and astrocytes. *Proceedings of the National Academy of Sciences of the United States of America, 113*(46), 13063-13068.

Mahmoud, S., Gharagozloo, M., Simard, C., & Gris, D. (2019). Astrocytes Maintain Glutamate Homeostasis in the CNS by Controlling the Balance between Glutamate Uptake and Release. *Cells, 8*(2), 184.

Mavelli, I., Ciriolo, M., & Rotilio, G. (1982). Superoxide dismutase, glutathione peroxidase and catalase in oxidative hemolysis. A Study of Fanconi's anemia

erythrocytes. *Biochemical and Biophysical Research Communications, 106*(2), 286-90.

McBean, G. J. (2018). Astrocyte Antioxidant Systems. *Antioxidants, 7*(112).

Pacey, L., Guan, S., Tharmalingam, S., Thomsen, C., & Hampson, D. (2015). Persistent astrocyte activation in the fragile X mouse cerebellum. *Brain and behaviour, 5*(10), e00400.

Pangrazzi, L., Balasco, L., & Bozzi, Y. (2020). Oxidative Stress and Immune System Dysfunction in Autism Spectrum Disorders. *International journal of molecular sciences, 21*(9), 3293.

Penagarikano, O., Mulle, J. G., & Warren, S. T. (2007). The Pathophysiology of Fragile X Syndrome. *The Annual Review of Genomics and Human Genetics, 8*, 109-29.

Raspa, M., Wheeler, A. C., & Riley, C. (2017, June). Public Health Literature Review of Fragile X Syndrome. *Pediatrics, 139*(3), e20161159.

Reinehr, R., Gorg, B., Becker, S., Qvartskhava, N., Bidmon, H., Selbach, O., . . . Haussinger, D. (2007). Hypoosmotic swelling and ammonia increase oxidative stress by NADPH oxidase in cultured astrocytes and vital brain slices. *Glia, 55*, 758-771.

Reynolds, I., & Hastings, T. (1995). Glutamate induces the production of reactive oxygen species in cultured forebrain neurons following NMDA receptor activation. *Journal of neuroscience, 15*(5 Pt 1), 3318-27.

Rizor, A., Pajarillo, E., Johnson, J., Aschner, M., & Lee, E. (2019). Astrocytic Oxidative/Nitrosative Stress Contributes to Parkinson's Disease Pathogenesis: The Dual Role of Reactive Astrocytes. *Antioxidants, 8*(8), 265.

675 Ross, M. A. (2000). Could oxidative stress be a factor in neurodevelopmental
676 disorders? *Prostalglandins, Leukotrienes and Essential Fatty Acids, 63*, 61-63.
677 Ross-Inta, C., Omanska-Klusek, A., Wong, S., Barrow, C., Garcia-Arocena, D.,
678 Iwahashi, C., . . . Giulivi, C. (2010). Evidence of mitochondrial dysfunction in
679 fragile X-associated tremor/ataxia syndrome. *Biochemical Journal, 429*(3), 545-
680 552.
681 Salim, S. (2017). Oxidative Stress and the Central Nervous System. *The Journal of*
682 *Pharmacology and Experimental Therapeutics, 360*, 201-205.

683 Schöpf, B., Schäfer, G., Weber, A., Talasz, H., Eder, I. E., Klocker, H., & Gnaiger, E.
684 (2016). Oxidative phosphorylation and mitochondrial function differ between human
685 prostate tissue and cultured cells. *The FEBS Journal*, *283*(11), 2181–2196.
686 https://doi.org/10.1111/febs.13733

687 Shanmugasundaram, K., Nayak, B., Friedrichs, W., Kaushik, D., Rodriguez, R., & Block,
688 K. (2017). NOX4 functions as a mitochondrial energetic sensor coupling cancer
689 metabolic reprogramming to drug resistance. *Nature communications, 997*.
690 Shen, M., Wang, F., Li, M., Sah, N., Stockton, M. E., Tidei, J. J., . . . Zhao, X. (2019).
691 Reduced mitochondrial fusion and Huntingtin levels contribute to impaired
692 dendritic maturation and behavioral deficits in Fmr1 mutant mice. *22*(3), 386-400.
693 Sorce, S., Stocker, R., Seredenina, T., Holmdahl, R., Aguzzi, A., Chio, A., . . . Jaquet, V.
694 (2017). NADPH oxidases as drug targets and biomarkers in neurodegenerative
695 diseases: What is the evidence? *Free radical biology & medicine, 112*, 387-396.

696 Stephen, T.-L., Gupta-Agarwal, S., & Kittler, J. T. (2014). Mitochondrial Dynamics in
697 astrocytes. *Biochemical Society Transactions, 42*(5).
698 Turrens, J. F. (2003). Mitochondrial formation of reactive oxygen species. *Journal of*
699 *Physiology*, 335-344.
700 Vallet, P., Charnay, Y., Steger, K., Ogier-Denis, E., Kovari, E., Herrmann, F., . . .
701 Szanto, I. (2005). Neuronal expression of the NADPH oxidase NOX4, and its
702 regulation in mouse experimental brain ischemia. *Journal of Neuroscience,*
703 *132*(2), 233-238.

704 Van Bergen, N., Blake, R., Crowston, J., & Trounce, I. (2014). Oxidative
705 phosphorylation measurement in cell lines and tissues. *Mitochondrion*, *15*.
706 https://doi.org/10.1016/j.mito.2014.03.003

707 Wallingford, J., Scott, A. L., Rodrigues, K., & Doering, L. C. (2017). Altered
708 Developmental Expression of the Astrocyte-Secreted Factors Hevin and
709 SPARC in the Fragile X Mouse Model. *Frontiers in Molecular Neuroscience*, *10*,
710 268. https://doi.org/10.3389/fnmol.2017.00268

711 Wang, S., Lim, S., Wang, Y., Lin, H., Lai, M., Ko, C., & Wang, J. (2018). Astrocytic
712 CCAAT/Enhancer-binding protein delta contributes to reactive oxygen species
713 formation in neuroinflammation. *Redox biology, 16*, 104-112.
714 Wang, Y., Branicky, R., Noe, A., & Hekimi, S. (2018). Superoxide dismutases: Dual
715 roles in controlling ROS damage and regulating ROS signaling. *Journal of cell*
716 *biology, 217*(6), 1915-1928.

Wilson, J. X. (1997). Antioxidant defense of the brain: a role for astrocytes. *Canadian Journal of Physiology and Pharmacology, 75*, 1149-1163.

Yuskaitis, C. J., Beurel, E., & Jope, R. S. (2010). Evidence of reactive astrocytes but not peripheral immune system activation in a mouse model of Fragile X syndrome. *Biochimica et biophysica acta, 1802*(11), 1006-12.

Zhao, R., Jiang, S., Zhang, L., & Yu, Z. (2019). Mitochondrial electron transport chain, ROS generation and uncoupling (Review). *International journal of molecular medicine, 44*(1), 3-15.

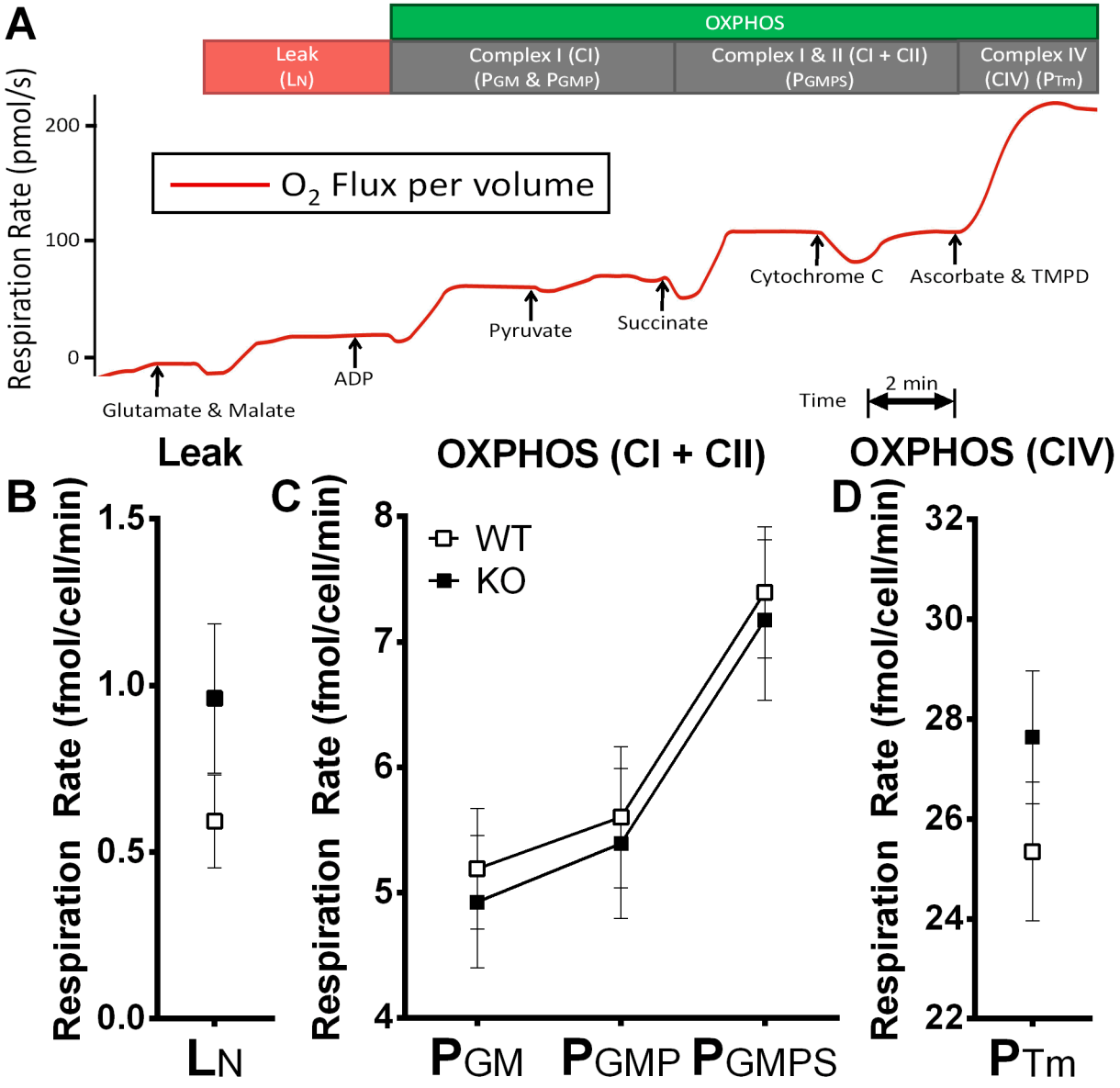

Figure 1. (*A*) Typical high resolution respirometry trace of WT oxygen consumption in permeabilized cultured astrocytes. Respiration rates of WT (n=13), and *Fmr*1 KO (n=14) permeabilized primary cortical astrocytes were stimulated via sequential application of exogenous substrates: addition of glutamate and malate for leak respiration (L_N); then ADP (P_{GM}) for oxidative phosphorylation via complex I; pyruvate (P_{GMP}) for maximal stimulation of complex I; succinate (P_{GMPS}) for stimulation of complex II; and finally, ascorbate and TMPD (P_{Tm}) for stimulation of complex IV. No differences in leak or oxidative phosphorylation capacity was measured between WT (white) and Fmr1 KO astrocytes (black; *B-D*). Error bars, SEM.

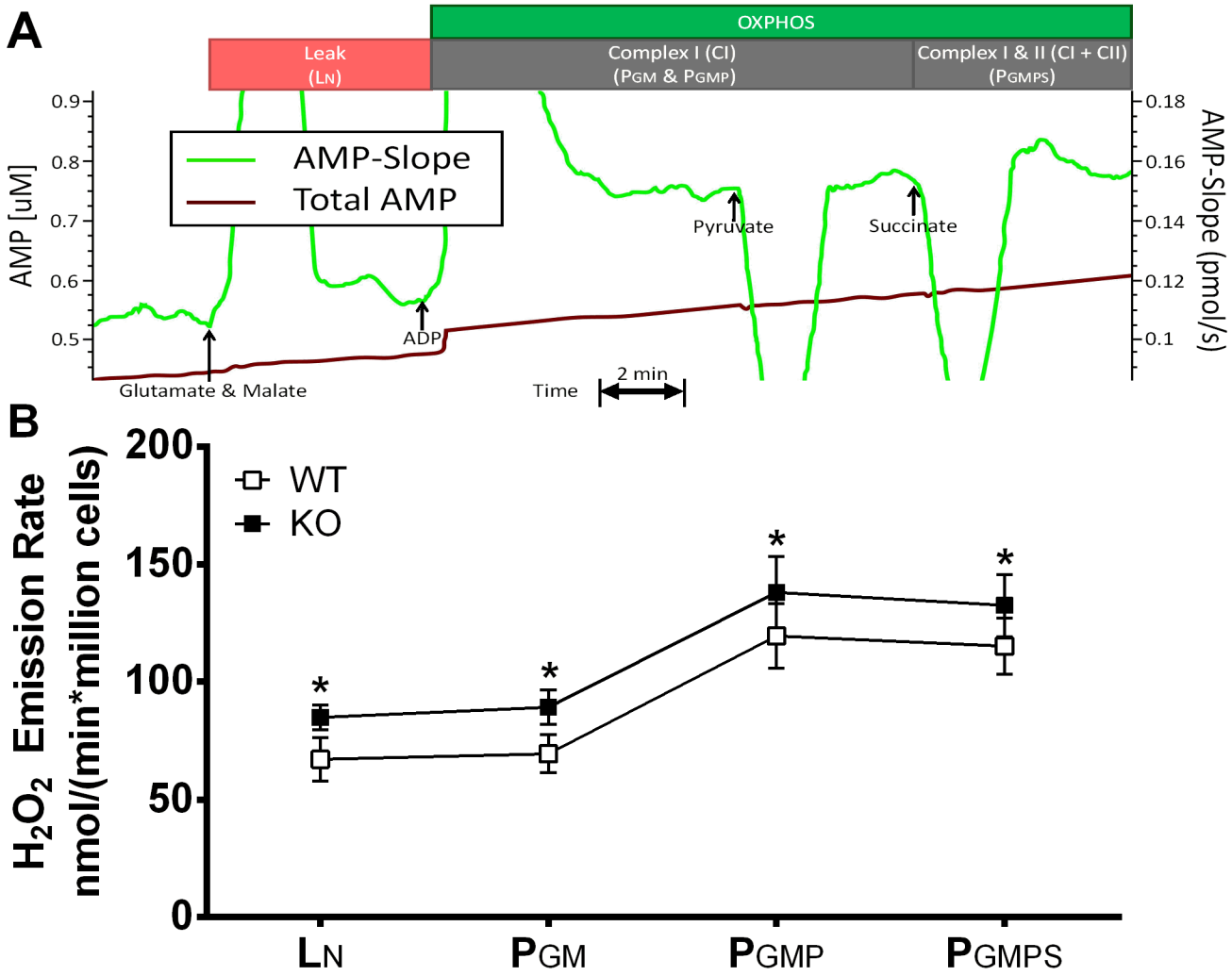

Figure 2. (*A*) Typical high resolution respirometry trace of WT H_2O_2 emissions in permeabilized cultured astrocytes. (*B*) H_2O_2 emission rates of WT (n=9) permeabilized primary cortical astrocytes were significantly lower than that of *Fmr*1 KO astrocytes (n=11). Respiration states were stimulated as previously stated: leak respiration (L_N) via glutamate and malate; oxidative phosphorylation of complex I with glutamate, malate, and ADP (P_{GM}); maximal stimulation of complex I with glutamate, malate, ADP, and pyruvate (P_{GMP}); and stimulation of complex II with glutamate, malate, ADP, pyruvate, and succinate (P_{GMPS}) *- Significant effect ($P<0.05$). Error bars, SEM.

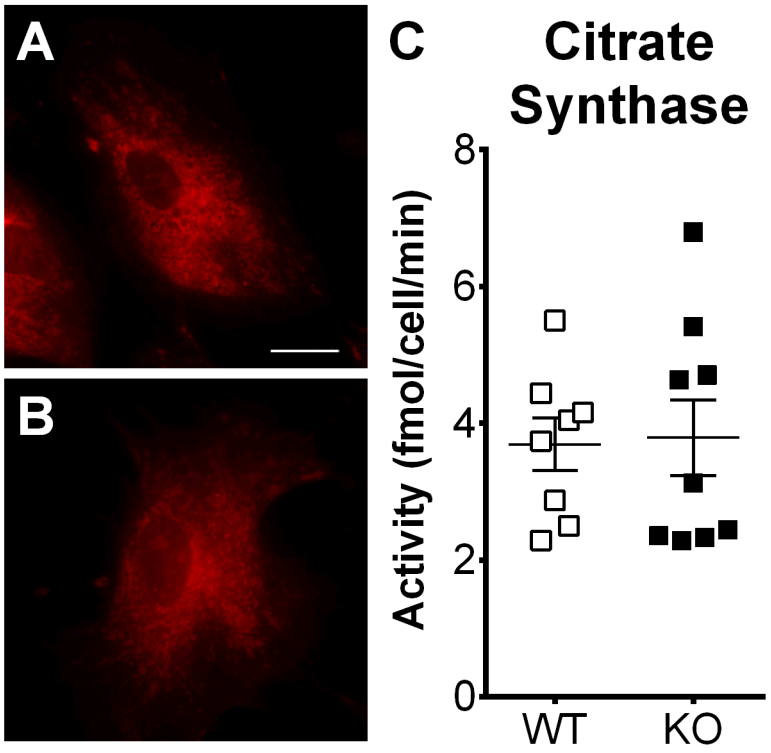

Figure 3. Representative images of WT (*A*) and *Fmr*1 KO (*B*) cortical cultured astrocytes stained with Mitotracker Red CMXRos. Scale bar, 20μm. (*C*) Activity of citrate synthase in WT (n=8) and Fmr1 KO (n=9) primary astrocytes. Astrocytes showed no significant genotypic difference in citrate synthase activity. Error bars, SEM.

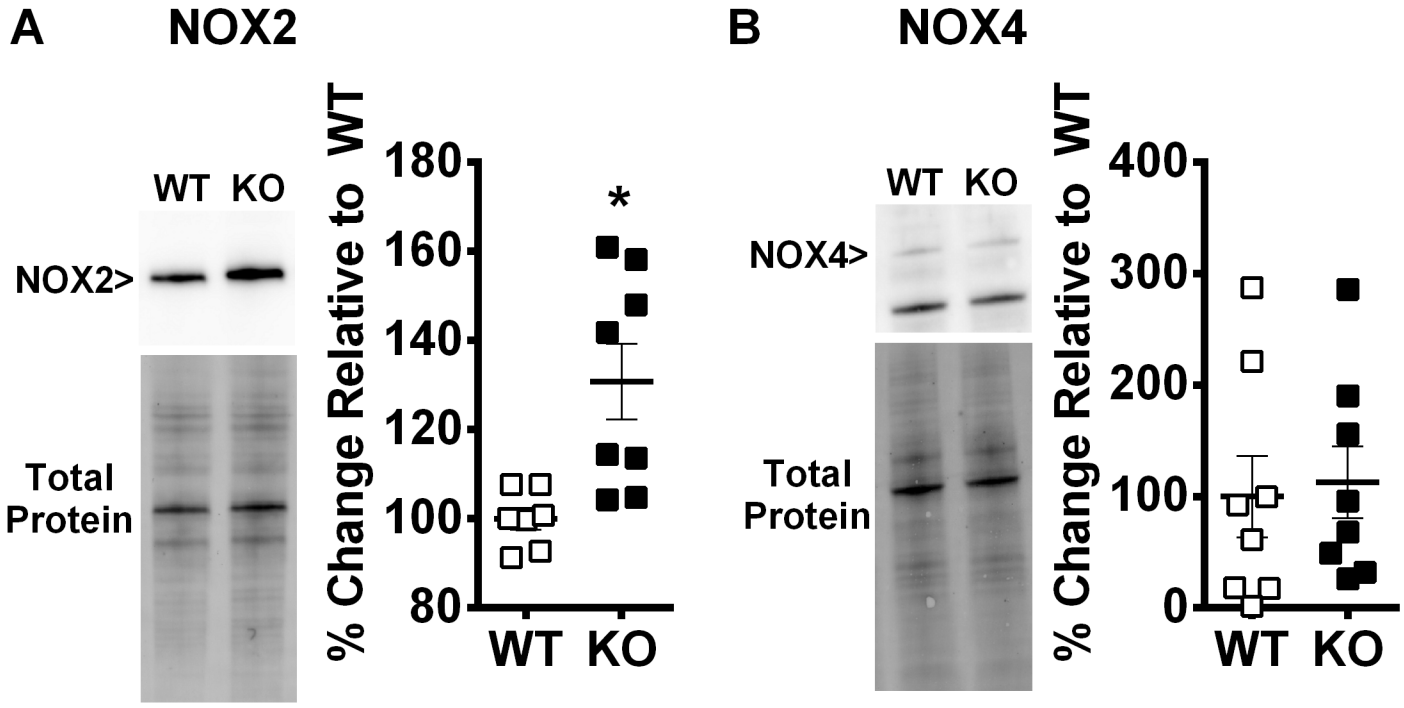

Figure 4. Protein expression of NADPH-oxidase (NOX) 2 and 4 in primary cortical astrocytes (n=7-8/group) isolated from *Fmr*1 KO mice. (A) NOX2 expression was elevated in Fmr1 KO (black) astrocytes compared to WT astrocytes (white). (B) There were no genotypic differences between WT and *Fmr*1 KO NOX4 expression. *- Significant effect ($P<0.05$). Error bars, SEM.

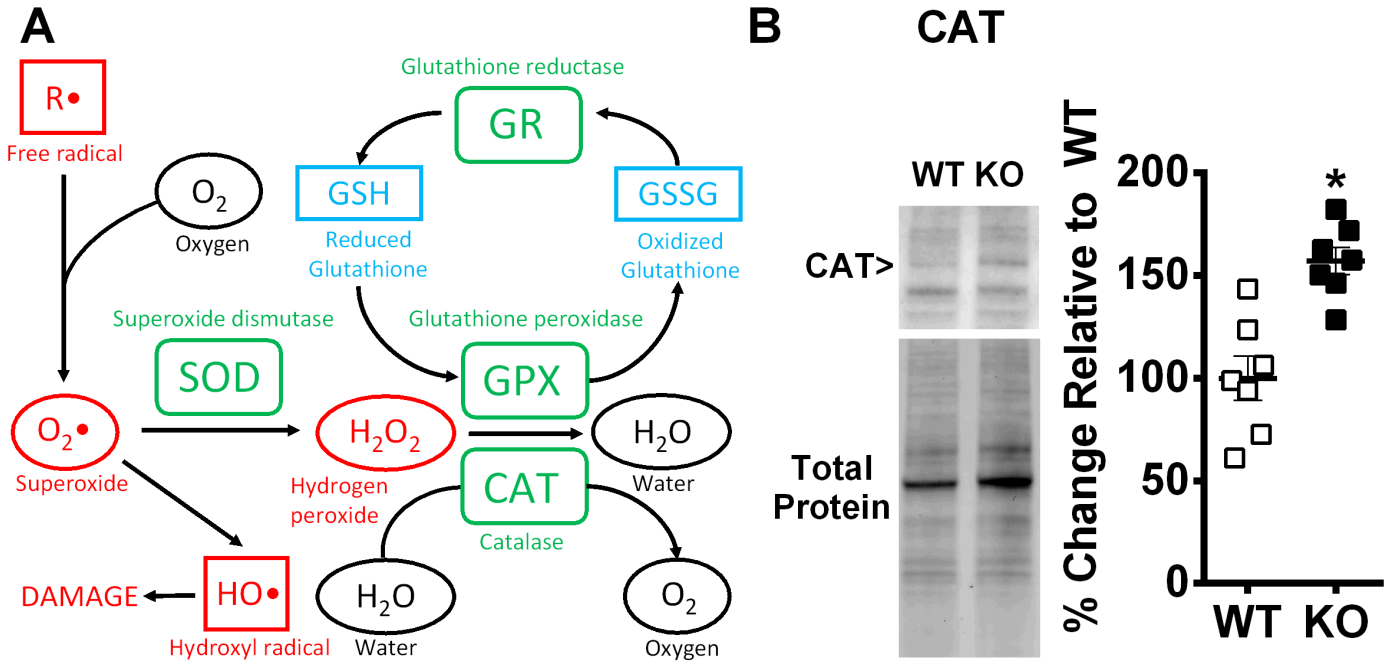

Figure 5. (*A*) Schematic of reactive oxygen species production and key antioxidant processes present in astrocytes to prevent oxidative damage. Protein expression of catalase in primary astrocytes (*B;* n=7/group) was elevated in *Fmr*1 KO (black) mice compared to WT (white). *- Significant effect ($P<0.05$). Error bars, SEM.

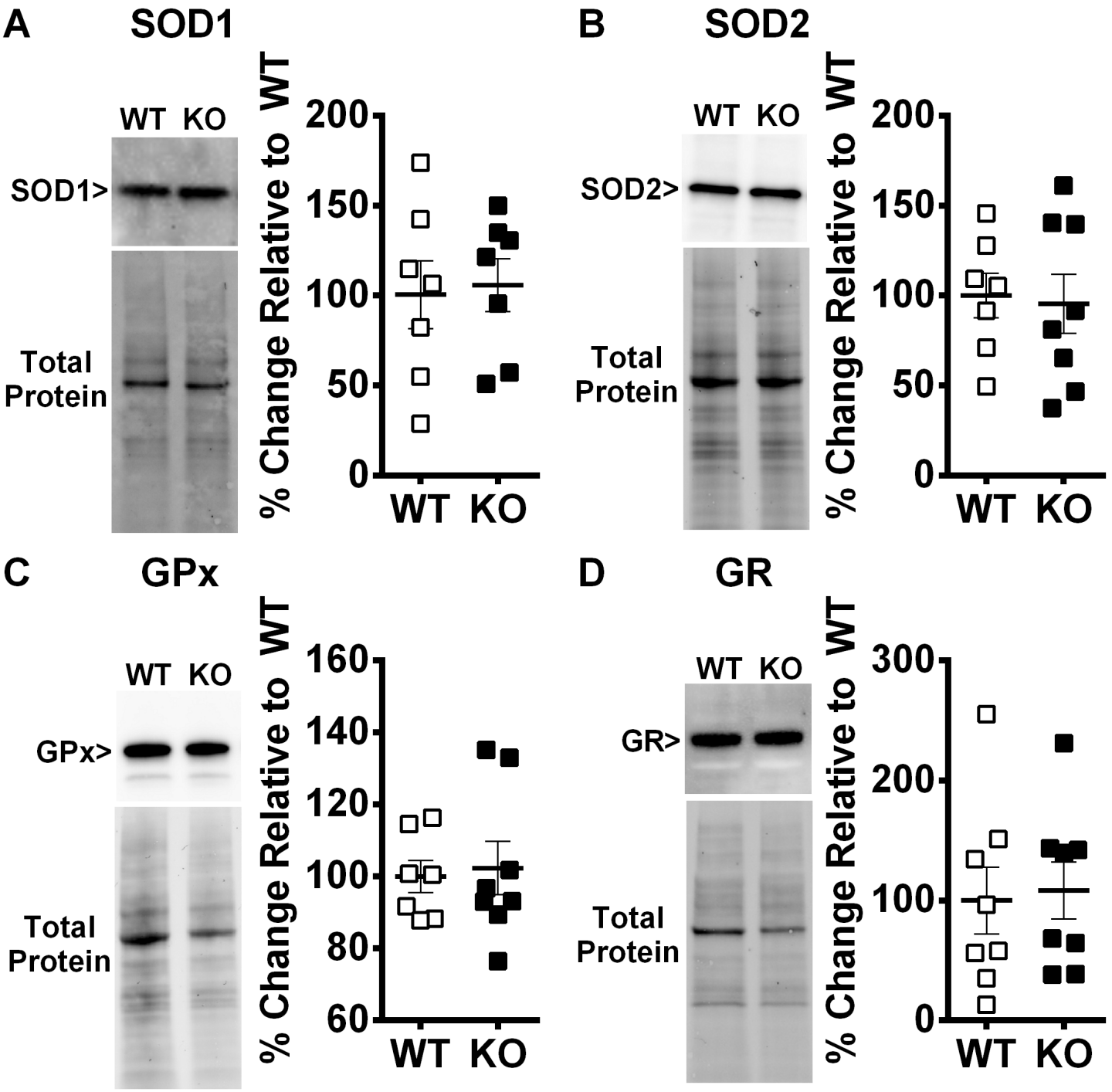

Figure 6. Protein expression of superoxide dismutase (SOD), glutathione peroxidase (GPx) and glutathione reductase (GR) antioxidant enzymes in WT and Fmr1 KO cultured primary astrocytes (n=7-8/group). No differences of SOD1 (A), SOD2 (B), GPx (C), or GR (D) were observed between WT (white) and *Fmr*1 KO (black) primary astrocytes. Error bars, SEM.